# Augmenting Neural Networks-Based Model Approximators in Robotic Force-Tracking Tasks

Kevin Saad<sup>1</sup> • Vincenzo Petrone<sup>2</sup> • Enrico Ferrentino<sup>2</sup> • Pasquale Chiacchio<sup>2</sup> • Francesco Braghin<sup>1</sup> • and Loris Roveda<sup>1,3</sup> • Francesco Braghin<sup>1</sup> • Pasquale Chiacchio<sup>2</sup> • Pasquale Chiacchio<sup></sup>

<sup>1</sup>Department of Mechanical Engineering, Politecnico di Milano, 20133 Milano, Italy

Keywords: Force Control, Robot-Environment Interaction, Neural Networks.

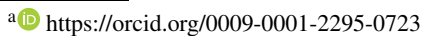
Abstract:

As robotics gains popularity, interaction control becomes crucial for ensuring force tracking in manipulator-based tasks. Typically, traditional interaction controllers either require extensive tuning, or demand expert knowledge of the environment, which is often impractical in real-world applications. This work proposes a novel control strategy leveraging Neural Networks (NNs) to enhance the force-tracking behavior of a Direct Force Controller (DFC). Unlike similar previous approaches, it accounts for the manipulator's tangential velocity, a critical factor in force exertion, especially during fast motions. The method employs an ensemble of feedforward NNs to predict contact forces, then exploits the prediction to solve an optimization problem and generate an optimal residual action, which is added to the DFC output and applied to an impedance controller. The proposed Velocity-augmented Artificial intelligence Interaction Controller for Ambiguous Models (VAICAM) is validated in the Gazebo simulator on a Franka Emika Panda robot. Against a vast set of trajectories, VAICAM achieves superior performance compared to two baseline controllers.

### 1 INTRODUCTION

Modeling and controlling accurate force tracking in robotic manipulators remains a fundamental challenge for reliable robot-environment interaction. Achieving high force-tracking performance is critical in a broad spectrum of tasks, including contact-rich manipulation, precision assembly, and surface interaction (see Fig. 1).

To address this challenge, impedance controllers achieve force-tracking accuracy through strategies such as reference generation (Roveda and Piga, 2021; Huang et al., 2022; Yu et al., 2024), variable stiffness (Shen et al., 2022; Li et al., 2023), and variable



b https://orcid.org/0000-0003-4777-1761

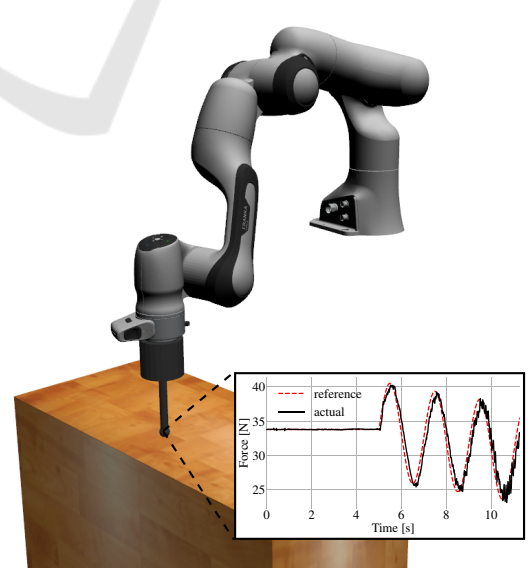


Figure 1: Simulation setup — the Panda robot performs a force-tracking task sliding on a wooden table with a spherical-tip end-effector.

<sup>&</sup>lt;sup>2</sup>Department of Information Engineering, Electrical Engineering and Applied Mathematics (DIEM), University of Salerno, 84084 Fisciano, Italy

<sup>&</sup>lt;sup>3</sup>Istituto Dalle Molle di Studi sull'Intelligenza Artificiale (IDSIA), Scuola Universitaria Professionale della Svizzera Italiana (SUPSI), Università della Svizzera Italiana (USI), 6962 Lugano, Switzerland

<sup>&</sup>lt;sup>c</sup> https://orcid.org/0000-0003-0768-8541

dip https://orcid.org/0000-0003-3385-8866

e https://orcid.org/0000-0002-0476-4118

f https://orcid.org/0000-0002-4427-536X

damping (Jung et al., 2004; Shu et al., 2021; Duan et al., 2018; Roveda et al., 2020). Reference generation methods implement an explicit direct force control (DFC) loop to follow a desired force trajectory, while variable impedance approaches often rely on simplified linear-spring environment models (Jung et al., 2004; Shen et al., 2022; Li et al., 2023; Shu et al., 2021; Duan et al., 2018; Yu et al., 2024). However, these simplified models typically represent only an approximation of the real environment dynamics (Roveda and Piga, 2021; Jung et al., 2004; Matschek et al., 2023).

To overcome modeling inaccuracies, recent literature has explored Artificial Intelligence (AI) techniques (Matschek et al., 2023), particularly Neural Networks (NNs), to learn a model-less, data-driven mapping between the manipulator's end-effector state and the exerted contact force directly at the control level. In this context, ORACLE (Petrone et al., 2025) was proposed as a controller that leverages NN-based models to optimize force tracking. However, ORACLE's original formulation neglects the effects of end-effector velocities tangential to the contact plane, potentially limiting its prediction accuracy and tracking performance, especially at high velocities.

This paper presents an extension of the ORA-CLE strategy by augmenting its model approximator's state with tangential velocity components, resulting in a refined controller named Velocity-Augmented Artificial Intelligence interaction Controller for Ambiguous Models (VAICAM). The proposed approach constructs an accurate model of the environment that relates the end-effector pose, penetration velocity, and tangential velocity to the resulting contact forces using feed-forward neural networks (FFNNs) (Nagabandi et al., 2018).

To this aim, a dedicated dataset containing dynamic trajectories in both force and position space is generated to train this model effectively. An improved controller is then designed based on this augmented model, enabling optimal selection of control actions to minimize force-tracking errors. Extensive validation is carried out in simulation, using Gazebo (Koenig and Howard, 2004), on a Franka Emika Panda manipulator (Haddadin et al., 2022). Furthermore, the paper conducts a comparative analysis between a standard direct force controller (Roveda and Piga, 2021) and ORACLE (Petrone et al., 2025) across varying velocity conditions, concretely attesting ORACLE's performance degradation as the endeffector velocity increases.

By integrating tangential velocity information into the ORACLE framework, VAICAM demonstrates improved force prediction and enhanced tracking capabilities, extending the applicability of neuralnetwork-based force controllers to a wider range of challenging interaction tasks.

#### 2 METHODOLOGY

This paper introduces VAICAM, an AI-driven tool to enhance the force tracking capabilities of an impedance controller used in unknown environments. It augments the ensemble of FFNNs originally proposed in ORACLE (Petrone et al., 2025) by adding to its input the tangential velocity v of the end-effector (EE), resulting in a mapping from the robot state and the DFC control action  $\mathbf{x}_f$  into its next state. This design choice yields a more accurate prediction of the next wrench, that will later be used to compute the optimal residual action added to the low-level control action of the DFC. VAICAM's overall control scheme is summarized in Fig. 2, whose building blocks will be detailed in the next sections.

#### 2.1 Base Controller

The low-level impedance controller enforces the desired interaction dynamics on the robot, specifically, Cartesian space mass-spring-damper dynamics. Consider the equations of motion for a manipulator with n Degrees of Freedom (DOFs) performing an m-dimensional task, with  $m \le 6 \le n$  (Featherstone and Orin, 2016):

$$m{B}(m{q})\ddot{m{q}} + m{C}(m{q}, \dot{m{q}})\dot{m{q}} + m{ au}_f(\dot{m{q}}) + m{g}(m{q}) = m{ au}_c - m{J}^{ op}(m{q})m{h}_e, \ (1)$$
 where  $m{B}(m{q}) \in \mathbb{R}^{n imes n}$  is the inertia matrix,  $m{C}(m{q}, \dot{m{q}}) \in$ 

where  $B(q) \in \mathbb{R}^{n \times m}$  is the inertia matrix,  $C(q,q) \in \mathbb{R}^{n \times n}$  is the matrix accounting for the centrifugal and Coriolis effects,  $\tau_f(\dot{q}) \in \mathbb{R}^n$  accounts for viscous and static friction,  $g(q) \in \mathbb{R}^n$  represents the torque exerted on the links by gravity,  $\tau_c \in \mathbb{R}^n$  indicates the torque control action,  $J(q) \in \mathbb{R}^{m \times n}$  is the geometric Jacobian, and  $h_e \in \mathbb{R}^m$  is the vector of wrenches exerted on the environment measured by means of a force/torque sensor mounted on the manipulator's flange. The vectors  $q, \dot{q}, \ddot{q} \in \mathbb{R}^n$  represent joint positions, velocities, and accelerations, respectively.

The expression of the Cartesian impedance control law with robot dynamics compensation is (Siciliano and Villani, 1999; Formenti et al., 2022)

$$\mathbf{\tau}_c = \mathbf{J}^{\top}(\mathbf{q})\mathbf{h}_c + \mathbf{C}(\mathbf{q}, \dot{\mathbf{q}})\dot{\mathbf{q}} + \mathbf{\tau}_f(\dot{\mathbf{q}}) + \mathbf{g}(\mathbf{q}), \quad (2)$$

where the task space wrench  $h_c$  realizing the compliant behavior can be chosen as (Caccavale et al., 1999; Iskandar et al., 2023)

$$\boldsymbol{h}_c = \boldsymbol{K}_d \Delta \boldsymbol{x} + \boldsymbol{D}_d \dot{\boldsymbol{x}}, \tag{3}$$

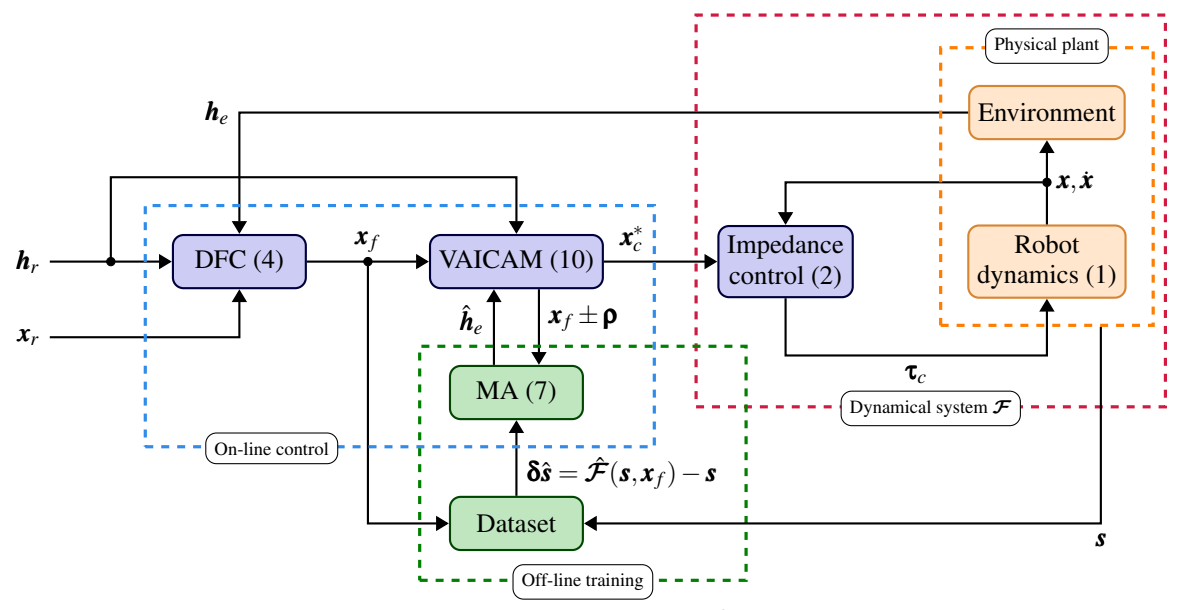


Figure 2: Control architecture. The MA learns the transition function  $\hat{\mathcal{F}}$  of the dynamical system represented by the impedance-controlled robot interacting with an unknown environment, given data composed of the system states  $\mathbf{s}$  and control inputs  $\mathbf{x}_f$ , i.e. the DFC action. After training, VAICAM computes the optimal residual action  $\mathbf{x}_c^*$ , aiming at minimizing the force tracking error between  $\mathbf{h}_r$  and the predicted wrench  $\hat{\mathbf{h}}_e$ .

where  $\mathbf{K}_d, \mathbf{D}_d \in \mathbb{R}^{m \times m}$  are diagonal matrices of control parameters, namely stiffness and damping, respectively, and  $\Delta \mathbf{x} \triangleq \mathbf{x}_d - \mathbf{x} \in \mathbb{R}^m$  is the Cartesian pose error between the setpoint  $\mathbf{x}_d \in \mathbb{R}^m$  and the actual robot pose  $\mathbf{x} \in \mathbb{R}^m$ . Assuming m = 6,  $\mathbf{x}$  is defined as  $\mathbf{x} \triangleq (x, y, z, \phi, \theta, \psi)^{\top}$ , where  $(x, y, z)^{\top}$  and  $(\phi, \theta, \psi)^{\top}$  are translational and rotational components, respectively.

### 2.2 Direct Force Controller

Given that the impedance controller solely manages interaction forces passively, lacking the capability to track a force reference, a DFC loop can be closed specifically along the directions in which force tracking is necessary (Roveda and Piga, 2021). The adopted control law is a simple PI controller having the following model:

$$\mathbf{x}_f = \mathbf{x}_r + \mathbf{\Gamma} \left( \mathbf{K}_P \Delta \mathbf{h} + \mathbf{K}_I \int_t \Delta \mathbf{h} dt \right),$$
 (4)

where, if m=6,  $\Gamma=\mathrm{diag}(\gamma_x,\gamma_y,\gamma_z,\gamma_\phi,\gamma_\theta,\gamma_\psi)$  is the task specification matrix (Khatib, 1987), with  $\gamma_i=1$  if the i-th direction is subject to force control, 0 otherwise.  $\boldsymbol{x}_f \in \mathbb{R}^m$  is the force controller output, while  $\boldsymbol{x}_r \in \mathbb{R}^m$  is the reference pose, whose i-th component is tracked when  $\gamma_i=0$ .  $\boldsymbol{K}_P,\boldsymbol{K}_I \in \mathbb{R}^{m \times m}$  are the proportional and integral gains of the controller, and  $\Delta \boldsymbol{h} = \boldsymbol{h}_r - \boldsymbol{h}_e \in \mathbb{R}^m$  is the error between the reference wrench to be exerted  $\boldsymbol{h}_r \in \mathbb{R}^m$  and the actual exerted wrench  $\boldsymbol{h}_e \in \mathbb{R}^m$ .

#### 2.3 Model Approximator

The Model Approximator (MA) addresses the inherent complications in accurately modeling the robot-environment interaction with a rather straightforward method that only requires the user to set up a handful of experiments that autonomously train the NN-based model. The MA deals with the current system state  $s_k$ , aiming to predict the state at the next time step k+1 following the equation

$$\hat{\boldsymbol{s}}_{k+1} = \hat{\boldsymbol{\mathcal{F}}}(\boldsymbol{s}_k, \boldsymbol{x}_f), \tag{5}$$

where  $\hat{\mathbf{s}}_{k+1}$  is the predicted next state.  $\hat{\mathcal{F}}$  represents the transition dynamics approximation which outputs the next predicted state, where  $\mathcal{F}$  indicates the actual dynamical system, i.e. the impedance-controlled robot (see Fig. 2). Specifically, instead of predicting  $\mathbf{s}_{k+1}$  explicitly, the actual FFNN's output  $\delta \hat{\mathbf{s}}$  is chosen to be the approximate difference between two subsequent states, similarly to (Nagabandi et al., 2018), i.e.:

$$\delta s = s_{k+1} - s_k. \tag{6}$$

This allows (5) to be rewritten as

$$\hat{\mathbf{s}}_{k+1} = \mathbf{s}_k + \mathbf{\delta}\hat{\mathbf{s}}(\mathbf{s}_k, \mathbf{x}_f), \tag{7}$$

with  $\delta \hat{s}(s_k, x_f)$  being the actual NN output, as in Fig. 3.

As regards the state definition, in general s takes the form

$$\mathbf{s} \triangleq (\mathbf{x}, \dot{\mathbf{x}}, \mathbf{h}_e)^{\top}, \tag{8}$$

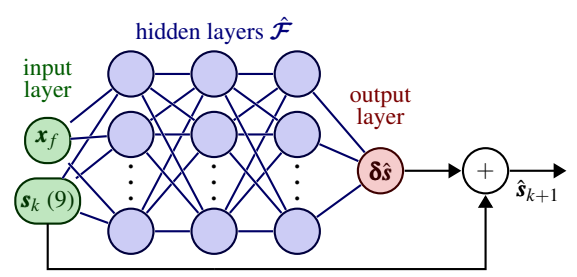


Figure 3: MA architecture. The hidden layers approximate the dynamics transition function  $\mathbf{s}_{k+1} = \mathcal{F}(\mathbf{s}_k, \mathbf{x}_f)$  by predicting the state variation  $\delta \hat{s}$ .

but it might be specialized according to the task setup. Indeed, assuming tracking forces only along the z axis, ORACLE (Petrone et al., 2025) only considers orthogonal components in s, i.e. EE penetration velocity and force along the same direction. This work introduces a new feature in s, namely the EE tangential velocity v, which influences the evolution of the exerted force, especially at high speeds (Iskandar et al., 2023). In summary, we propose the following augmentation in the MA state representation:

$$\mathbf{s} \triangleq (z, \dot{z}, f_z)^{\top} \to \mathbf{s} \triangleq (z, \dot{z}, v, f_z)^{\top}, \tag{9}$$

where  $v = \sqrt{\dot{x}^2 + \dot{y}^2}$  is the tangential velocity, with  $\dot{x}$ ,  $\dot{y}$  being the velocity components on the EE xy plane, and  $f_z$  is the normal force along z, i.e., the contact

From an architectural standpoint, the FFNN is actually an ensemble of FFNN as in (Chua et al., 2018), since using an array of N independently trained NNs minimizes the errors risen by epistemic and stochastic uncertainties.

#### 2.4 VAICAM Algorithm

Acting as the glue that joins all items together, the VAICAM algorithm combines the DFC-enhanced impedance controller and the MA. It utilizes the control action output by the DFC  $x_f$  along with the force prediction of the MA  $\hat{h}_e$ , and then outputs the optimal residual action  $\mathbf{x}_{c}^{*}$  that will then be added to the impedance controller action aiming at minimizing the force tracking error. VAICAM will search for  $\mathbf{x}_c^*$  in the neighborhood of  $x_f$  in an area centered around it with predefined radius  $\rho > 0$ .

Then, the control input to the impedance controller is updated by solving an optimization problem, run at each control step k:

$$\boldsymbol{x}_{c}^{*}(k) = \underset{\boldsymbol{x}_{c} \in \boldsymbol{x}_{f} \pm \boldsymbol{\rho}}{\arg\min} \mathcal{L}_{k}(\boldsymbol{s}, \boldsymbol{x}_{c}, \boldsymbol{h}_{r}), \tag{10}$$

where

$$\mathcal{L}_k(\boldsymbol{s}, \boldsymbol{x}_c, \boldsymbol{h}_r) = |\boldsymbol{h}_r(k) - \hat{\boldsymbol{h}}_e(\boldsymbol{s}_k, \boldsymbol{x}_c)| + \Omega_k(\boldsymbol{x}_c) \quad (11)$$

```
Data: \boldsymbol{x}_f from (4), \boldsymbol{s} = (\boldsymbol{x}, \dot{\boldsymbol{x}}, \boldsymbol{h}_e)^{\top}, \boldsymbol{h}_r
       Result: x_c^*
       if k = 1 then
               Set \alpha, \beta and \rho;
               Set weights of the pre-trained MA NN
                  ensemble:
       end
       Build the discretized neighborhood of candidate
          optimal actions \boldsymbol{B}_{\boldsymbol{\rho}}(\boldsymbol{x}_f) = [\boldsymbol{x}_f \pm \boldsymbol{\rho}];
       for x_c \in B_0(x_f) do
               Infer the predicted force from the model
                  approximator with (7):
                  \hat{\boldsymbol{h}}_e(\boldsymbol{s},\boldsymbol{x}_c) = \boldsymbol{h}_e + \boldsymbol{\delta}\hat{\boldsymbol{h}}_e(\boldsymbol{s},\boldsymbol{x}_c);
               Compute the regularizer in (12) as
                  \Omega_k(\mathbf{x}_c) = \|\mathbf{x}_c\|_{\mathbf{\alpha}}^2 + |\mathbf{x}_c - \mathbf{x}_c^*(k-1)|_{\mathbf{\beta}};
               Compute the corresponding loss function in
                  (11) as \mathcal{L}_k(\boldsymbol{s}, \boldsymbol{x}_c, \boldsymbol{h}_r) = |\boldsymbol{h}_r - \hat{\boldsymbol{h}}_e| + \Omega_k(\boldsymbol{x}_c);
       end
       Call VAICAM by solving the optimization
         problem in (10) minimizing (11):
         \mathbf{x}_c^*(k) = \operatorname{arg\,min}_{\mathbf{x}_c \in \mathbf{B}_{\mathbf{p}}(\mathbf{x}_f)} \mathcal{L}_k(\mathbf{s}, \mathbf{x}_c, \mathbf{h}_r);
Algorithm 1: VAICAM algorithm at every control
step k.
```

is the cost function to minimize, whose first term  $|\boldsymbol{h}_r \hat{\mathbf{h}}_{e}$  is the expected force tracking error, and

$$\Omega_k(\mathbf{x}_c) = \|\mathbf{x}_c\|_{\alpha}^2 + |\mathbf{x}_c - \mathbf{x}_c^*(k-1)|_{\beta}$$
 (12)

is a regularizer that contributes to smoothing-out large jumps of the control term  $x_c$ . The first term in (12) penalizes heavy actions so as to avoid deep penetrations of the EE into the environment, whereas the second prevents fast variations between subsequent actions. The two terms are defined as:

$$\|\boldsymbol{x}_c\|_{\boldsymbol{\alpha}}^2 = \sum_{i} \alpha_i x_{c,i}^2, \tag{13a}$$

$$\|\mathbf{x}_{c}\|_{\alpha}^{2} = \sum_{i} \alpha_{i} x_{c,i}^{2},$$

$$|\mathbf{x}_{c} - \mathbf{x}_{c}^{*}(k-1)|_{\beta} = \sum_{i} \beta_{i} |x_{c,i} - x_{c,i}^{*}(k-1)|,$$
(13a)

where both  $\alpha, \beta \in \mathbb{R}^m$  are parameters to be chosen by the user. This method, summarized in Algorithm 1, along with the base force controller, is activated as soon as contact is established between the EE and the environment.

#### **Training Procedure** 2.5

The training and validation of the ensemble of FFNN, which is done in a preliminary offline stage, uses collected data resulting from thorough exploration of the state space. In order to collect the data, reference forces and positions are provided to the base force controller, and the output data, consisting of the actual robot states s and control actions  $x_f$ , are recorded. During the training stage of the FFNN, their weights are updated using the Stochastic Gradient Descent algorithm in order to minimize the Mean Squared Error (MSE) between the actual and estimated states.

In our training procedure, we recommend commanding sine waves as references in both force and position spaces, in order to have a thorough exploration and avoid data gaps in the state domain. Commanding a sine wave reference for the position additionally entails that the EE velocity v is sinusoidal, allowing for the complete exploration of the velocity space as well. This is a crucial aspect because, compared to (Petrone et al., 2025), the inclusion of the new feature v requires a dedicated training. Furthermore, we recommend exaggerating the amplitude of the sine wave force references: even though they cannot be perfectly tracked by the controller, this ensures that the force domain is sufficiently explored.

After collecting data, they are then processed following methods used in (Nagabandi et al., 2018; Chua et al., 2018), i.e. they are normalized by subtracting the mean of each quantity and then dividing by its standard deviation. A zero-mean Gaussian noise in the form  $\mathcal{N}(\mu=0,\sigma)$  is applied to the measured data  $h_e$  in order to enhance the robustness of the NN.

#### 3 RESULTS

#### 3.1 Task and Materials

The experimental validation is divided into two main phases, both conducted on the 7-DOF Franka Emika Panda robot:

- Experiment I: train, validate, and test the Static Model Approximator (SMA) used by ORACLE, which is the MA trained and validated using *static* position references (Petrone et al., 2025) *without* tangential velocity, and the Dynamic Model Approximator (DMA) used by VAICAM, which is the MA trained and validated using *dynamic* position references *with* tangential velocities;
  - the goal is to assess the performance of both MAs on dynamic position reference trajectories, and validate that the DMA yields higher accuracy as the tangential velocity increases;
- Experiment II: execute dynamic trajectories using the base controller (Roveda and Piga, 2021), ORACLE (Petrone et al., 2025) and VAICAM, and compare the force tracking results;
  - in this case, the objective is to assess the performance of both control strategies, and validate that the controller that uses the DMA (VAICAM) performs better than both the base

Table 1: Parameters used in the experiments.

Parameter	Value
Coulomb friction coefficient $\mu$	0.2
Time step solver	ODE
Impedance control translational stiffness $K_{d,t}$	1700
Impedance control orientational stiffness $K_{d,r}$	300
Damping ratio ξ	1
DFC Proportional gain $K_P$	$\begin{array}{ c c c c }\hline 1 \cdot 10^{-6} \\ 2 \cdot 10^{-3} \\ \hline \end{array}$
DFC Integral gain $K_I$	$2 \cdot 10^{-3}$

Table 2: Configurations of the FFNN ensemble.

Parameter	Value
Number of estimators <i>N</i>	3
Hidden layers	3
Neurons per layer	200
Activation function	ReLU
Learning rate	$1 \cdot 10^{-3}$
Ensemble type	Fusion
Training epochs	50
Loss function	MSE
Weight optimizer	Adam

controller and the controller that uses the SMA (ORACLE).

The NN's algorithm is coded in Python using PyTorch (Paszke et al., 2019), interfacing with the other modules via ROS communication mechanisms (Quigley et al., 2009). The controllers implemented in ROS are coded in C++.

In order to accurately simulate the robot, Gazebo (Koenig and Howard, 2004) is used as the simulation software. A spherical tip EE is mounted at the flange of the robot (see Fig. 1). The interaction control parameters are chosen as  $\mathbf{K}_d = \mathrm{diag}(K_{d,t}, K_{d,t}, K_{d,t}, K_{r,t}, K_{r,t}, K_{r,t})$  and  $\mathbf{D}_d = \mathrm{diag}\{\xi\sqrt{K_{d,i}}\}_{i=1}^6$ , where  $K_{d,t}$  and  $K_{d,r}$  are the translational and rotational stiffness gains, respectively, and  $\xi$  is the damping ratio. Table 1 provides a summary of the parameters. In our experiment, a linear force is exerted on the z axis, thus  $\Gamma = \mathrm{diag}(0,0,1,0,0,0)$ .

## 3.2 Experiment I: Model Approximator Validation

For a fair comparison with (Petrone et al., 2025), we base the FFNNs structure on the findings therein. Specifically, all FFNNs used share the same configuration in terms of depth (number of hidden layers), width (number of neurons per layer) and learning algorithm parameters, as listed in Table 2. Linear type layers are used, while the activation function is of the ReLU type (Agarap, 2019). The optimized configuration of the base estimator that ensures enhanced inference time without compromising prediction ac-

curacy uses N=3 FFNNs. Adam (Kingma and Ba, 2015) refers to Adaptive Moment Estimation, an optimizer used for NN regression tasks, while "Fusion" indicates how a single output is retrieved from the ensemble, i.e. the arithmetic average across the independent network estimations is computed.

#### 3.2.1 Static Model Approximator

The dataset is composed of 10 trajectories, with 9 of them being used in the training set, and the remaining 1 in the validation set, used by Adam (Kingma and Ba, 2015) to adaptively optimize the learning rate. The position reference is in the form of a static waypoint, as this MA, unlike the one proposed in this work, does not take into consideration  $\nu$  (Petrone et al., 2025). The force reference is in the form of a sinusoidal wave with randomized frequency, amplitude, and mean. Raw data in both training and validation sets are pre-processed as indicated in Sect. 2.5.

After training the MA, a test set is developed in order to assess its performance. Since the aim of this work is to assess the MA generalization ability against dynamic position trajectories, this set is composed of horizontal line references that the EE tries to track with a constant velocity and a sinusoidal force reference. The MA is tested against a total of 110 trajectories of about 1.2 m executed using the base controller, divided into 11 evenly-spaced velocities in the range [0.01,0.50] m/s. The performance assessment is based on the comparison of the force predicted by the MA with the actual force.

#### 3.2.2 Dynamic Model Approximator

Compared to the SMA discussed in Sect. 3.2.1, we adopt a different training approach, i.e. both the force and position references in the training set take a sinusoidal form. On the basis of the training procedure outlined in Sect. 2.5, sinusoidal position references allow covering the desired velocity span better than constant velocity profiles. The validation set is composed of 11 trajectories, each randomly given a velocity from the 11 velocity samples in the range [0.01, 0.50] m/s.

After executing the trajectories, the data stored in the dataset are pre-processed according to the procedure reported in Sect. 2.5. Using the DMA, the network now takes into consideration  $\nu$  while predicting the next state, which ameliorates the performance of the MA at higher velocities. In order to confirm this thesis, the DMA is evaluated on the same test set as the SMA's, i.e. using the same 110 line trajectories.

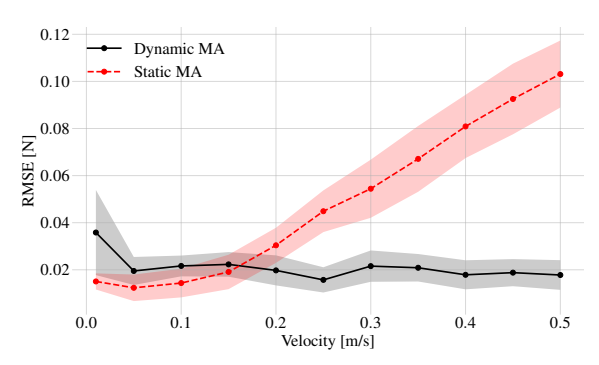


Figure 4: Comparison between the static and the dynamic model approximators, in terms of RMSE, as the EE velocity increases.

Table 3: Average RMSE of static and dynamic model approximators across trajectories —  $\eta$  indicates the improvement factor of DMA over SMA.

	Velocity	RMS	n	
	[m/s]	SMA	<b>DMA</b>	η
	0.01	0.0154	0.0397	0.3877
	0.05	0.0135	0.0203	0.663
)	0.1	0.0155	0.022	0.7029
	0.15	0.0203	0.0228	0.8893
	0.2	0.0312	0.0207	1.511
	0.25	0.0456	0.0165	2.7628
	0.3	0.0557	0.0225	2.4777
	0.35	0.0684	0.0216	3.1683
1	0.4	0.0819	0.0188	4.3528
	0.45	0.0936	0.0196	4.7841
)	0.5	0.104	0.0188	5.5422

#### 3.2.3 Model Approximators Comparison

Fig. 4 reports the Root Mean Square Error (RMSE) between the predicted and measured force, when either the SMA or DMA is employed, for increasing EE tangential velocity  $\nu$ . As expected, the plot reveals a better generalization ability of the DMA over the SMA to higher EE velocities. While the results are comparable at low speed, as  $\nu$  increases the SMA showcases lower prediction accuracy, in terms of both mean and variance across trajectories.

This qualitative analysis is quantitatively confirmed by Table 3, which also reports the numerical improvement factor  $\eta$  of DMA over SMA. As  $\nu$  increases, the former outperforms the latter by up to 454%, in terms of average RMSE recorded across trajectories at the same velocity.

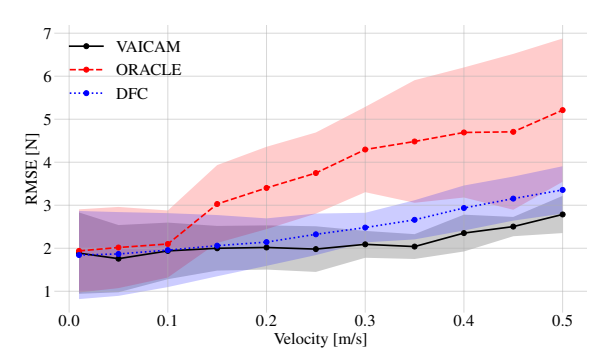


Figure 5: Comparison between the baseline DFC (Roveda and Piga, 2021), ORACLE (Petrone et al., 2025), and VAICAM (ours), in terms of RMSE, as the EE velocity increases.

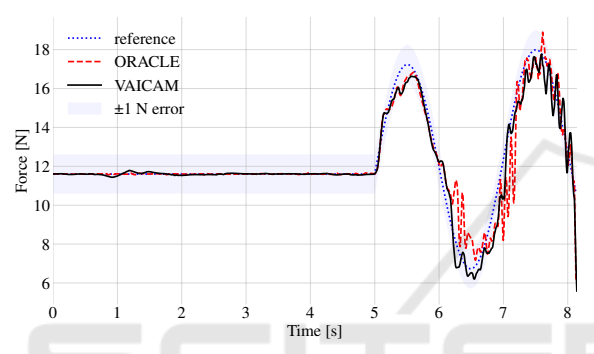


Figure 6: Force tracking comparison between ORACLE (Petrone et al., 2025) and VAICAM (ours) at  $v = 0.2 \,\text{m/s}$ .

## 3.3 Experiment II: Control Algorithm Validation

Once the SMA and the DMA are trained, the three control algorithms — DFC (Roveda and Piga, 2021), ORACLE (Petrone et al., 2025), and VAICAM (ours) — can be tested against a test set aiming to prove that VAICAM outperforms its competitors. The optimizer parameters are tuned as  $\alpha=25,\ \beta=200,\ \text{and}\ \rho=0.003\,\text{m}$  for both ORACLE and VAICAM.

As can be seen from Fig. 5, the average force-tracking RMSE for VAICAM is approximately constant for  $v \in [0,0.35]$  m/s, and starts increasing for v > 0.35 m/s. Thanks to the exploitation of the novel DMA, VAICAM outperforms both ORACLE and the base DFC. A sample trajectory is considered in Fig. 6, visually showing that ORACLE's uncertainty at moderate velocities (due to the limited SMA) translates into worse force-tracking capabilities. Furthermore, Fig. 5 shows that VAICAM also enhances the DFC performance, although with a lower improvement factor compared to ORACLE. Lastly, it is worth noticing that VAICAM's RMSE standard deviation is lower than DFC's, thus manifesting a superior robustness w.r.t. the experimental conditions.

Table 4: Average RMSE of baseline DFC (Roveda and Piga, 2021), ORACLE (Petrone et al., 2025), and VAICAM (ours) across trajectories —  $\eta$  indicates the improvement factor of VAICAM over DFC or ORACLE.

Velocity	RMSE [N]			η	
[m/s]	DFC	ORACLE	VAICAM	DFC	ORACLE
0.01	2.0579	2.1222	2.0676	0.9953	1.0264
0.05	2.0602	2.1867	1.8917	1.0891	1.1559
0.1	2.1022	2.2118	2.0259	1.0377	1.0918
0.15	2.1563	3.135	2.0528	1.0504	1.5272
0.2	2.199	3.5081	2.0697	1.0624	1.695
0.25	2.3638	3.8424	2.0362	1.1609	1.887
0.3	2.4995	4.3858	2.1098	1.1847	2.0788
0.35	2.6919	4.6601	2.0553	1.3097	2.2673
0.4	2.973	4.883	2.3837	1.2472	2.0485
0.45	3.1873	4.978	2.5117	1.269	1.982
0.5	3.3923	5.4201	2.8123	1.2062	1.9273

To confirm the improvement of VAICAM over both DFC and ORACLE, Table 4 displays the numerical results by reporting the average RMSE of these 3 strategies for each velocity. As  $\eta$  confirms, VAICAM surpasses the DFC by up to 31% (at  $\nu = 0.35\,\text{m/s}$ ), while the improvement over ORACLE at maximum experimental speed ( $\nu = 0.5\,\text{m/s}$ ) reaches 127%.

#### 4 CONCLUSIONS

This paper introduced VAICAM, a controller improving the state-of-the-art of robot-environment interaction tasks that require dynamic trajectories. It makes use of an FFNN ensemble that acts as a model approximator considering the tangential velocity of the EE. The controller is based on an impedance controller to ensure a compliant behavior, and a DFC to guarantee the desired force tracking characteristics. An ensemble of FFNNs is developed, trained, and tested along the work. The networks are able to predict the force that the manipulator will exert on the environment, allowing the computation of an optimal residual action. The latter is then added to the action of a baseline DFC to improve its force-tracking capabilities, by correcting the next commanded position. Tested in a simulated environment, VAICAM outperformed the baseline DFC (Roveda and Piga, 2021) and a similar algorithm from recent literature (Petrone et al., 2025).

Possible future improvements of the proposed strategy are: (i) extending the comparison with other controllers from the literature, e.g. (Iskandar et al., 2023); (ii) assessing whether these controllers can benefit from a MA like the one developed in this work to improve their performance; (iii) deploying the algorithm on real hardware, for a complete validation of VAICAM's performance; (iv) extending the state space to include tangential position components, to tackle variable-stiffness environments; (v) including the DMA in optimal planning algo-

rithms foreseeing robot-environment interaction trajectories (Petrone et al., 2022).

#### **REFERENCES**

- Agarap, A. F. (2019). Deep Learning using Rectified Linear Units (ReLU). arXiv preprint: 1803.08375.
- Caccavale, F., Natale, C., Siciliano, B., and Villani, L. (1999). Six-DOF impedance control based on angle/axis representations. *IEEE Trans. Robot. Au*tomat., 15(2):289–300.
- Chua, K., Calandra, R., McAllister, R., and Levine, S. (2018). Deep Reinforcement Learning in a Handful of Trials using Probabilistic Dynamics Models. In Adv. Neural Inform. Process. Syst., volume 32, pages 4754–4765.
- Duan, J., Gan, Y., Chen, M., and Dai, X. (2018). Adaptive variable impedance control for dynamic contact force tracking in uncertain environment. *Robot. Auton. Syst.*, 102:54–65.
- Featherstone, R. and Orin, D. E. (2016). Dynamics. In Siciliano, B. and Khatib, O., editors, *Springer Handbook of Robotics*, volume 3, pages 195–211. Springer, 2 edition.
- Formenti, A., Bucca, G., Shahid, A. A., Piga, D., and Roveda, L. (2022). Improved impedance/admittance switching controller for the interaction with a variable stiffness environment. *Compl. Eng. Syst.*, 2(3). Art. no. 12.
- Haddadin, S., Parusel, S., Johannsmeier, L., Golz, S., Gabl, S., Walch, F., Sabaghian, M., Jähne, C., Hausperger, L., and Haddadin, S. (2022). The Franka Emika Robot: A Reference Platform for Robotics Research and Education. *IEEE Robot. Automat. Mag.*, 29(2):46–64.
- Huang, H., Guo, Y., Yang, G., Chu, J., Chen, X., Li, Z., and Yang, C. (2022). Robust Passivity-Based Dynamical Systems for Compliant Motion Adaptation. *IEEE/ASME Trans. Mechatron.*, 27(6):4819–4828.
- Iskandar, M., Ott, C., Albu-Schäffer, A., Siciliano, B., and Dietrich, A. (2023). Hybrid Force-Impedance Control for Fast End-Effector Motions. *IEEE Robot. Automat. Lett.*, 8(7):3931–3938.
- Jung, S., Hsia, T. C. S., and Bonitz, R. G. (2004). Force Tracking Impedance Control of Robot Manipulators Under Unknown Environment. *IEEE Trans. Contr. Syst. Technol.*, 12(3):474–483.
- Khatib, O. (1987). A unified approach for motion and force control of robot manipulators: The operational space formulation. *IEEE J. Robot. Automat.*, 3(1):43–53.
- Kingma, D. P. and Ba, J. (2015). Adam: A Method for Stochastic Optimization. In *Int. Conf. Learn. Repre*sent.
- Koenig, N. and Howard, A. (2004). Design and Use Paradigms for Gazebo, an Open-Source Multi-Robot Simulator. In *IEEE Int. Conf. Intell. Robots Syst.*, volume 3, pages 2149–2154.

- Li, K., He, Y., Li, K., and Liu, C. (2023). Adaptive fractional-order admittance control for force tracking in highly dynamic unknown environments. *Int. J. Robot. Res. Applic.*, 50(3):530–541.
- Matschek, J., Bethge, J., and Findeisen, R. (2023). Safe Machine-Learning-Supported Model Predictive Force and Motion Control in Robotics. *IEEE Trans. Contr. Syst. Technol.*, 31(6):2380–2392.
- Nagabandi, A., Kahn, G., Fearing, R. S., and Levine, S. (2018). Neural Network Dynamics for Model-Based Deep Reinforcement Learning with Model-Free Fine-Tuning. In *IEEE Int. Conf. Robot. Automat.*, pages 7559–7566.
- Paszke, A., Gross, S., Massa, F., Lerer, A., Bradbury, J., Chanan, G., Killeen, T., Lin, Z., Gimelshein, N., Antiga, L., Desmaison, A., Köpf, A., Yang, E., De-Vito, Z., Raison, M., Tejani, A., Chilamkurthy, S., Steiner, B., Fang, L., Bai, J., and Chintala, S. (2019).
  PyTorch: An Imperative Style, High-Performance Deep Learning Library. In Adv. Neural Inform. Process. Syst., volume 33, pages 8026–8037.
- Petrone, V., Ferrentino, E., and Chiacchio, P. (2022). Time-Optimal Trajectory Planning With Interaction With the Environment. *IEEE Robot. Automat. Lett.*, 7(4):10399–10405.
- Petrone, V., Puricelli, L., Pozzi, A., Ferrentino, E., Chiacchio, P., Braghin, F., and Roveda, L. (2025). Optimized Residual Action for Interaction Control with Learned Environments. *IEEE Trans. Contr. Syst. Technol.* Accepted for publication.
- Quigley, M., Conley, K., Gerkey, B., Faust, J., Foote, T., Leibs, J., Wheeler, R., and Ng, A. (2009). ROS: an open-source Robot Operating System. In *IEEE Int. Conf. Robot. Automat.*, volume 3.
- Roveda, L., Castaman, N., Franceschi, P., Ghidoni, S., and Pedrocchi, N. (2020). A Control Framework Definition to Overcome Position/Interaction Dynamics Uncertainties in Force-Controlled Tasks. In *IEEE Int. Conf. Robot. Automat.*, pages 6819–6825.
- Roveda, L. and Piga, D. (2021). Sensorless environment stiffness and interaction force estimation for impedance control tuning in robotized interaction tasks. *Auton. Robots*, 45(3):371–388.
- Shen, Y., Lu, Y., and Zhuang, C. (2022). A fuzzy-based impedance control for force tracking in unknown environment. *J. Mech. Sci. Technol.*, 36(10):5231–5242.
- Shu, X., Ni, F., Min, K., Liu, Y., and Liu, H. (2021). An Adaptive Force Control Architecture with Fast-Response and Robustness in Uncertain Environment. In *Int. Conf. Robot. Biom.*, pages 1040–1045.
- Siciliano, B. and Villani, L. (1999). Indirect Force Control. In *Robot Force Control*, pages 31–64. Springer US.
- Yu, X., Liu, S., Zhang, S., He, W., and Huang, H. (2024). Adaptive Neural Network Force Tracking Control of Flexible Joint Robot With an Uncertain Environment. *IEEE Trans. Ind. Electron.*, 71(6):5941–5949.